Spectral Analysis of GFDM Modulated Signal under Nonlinear Behavior of Power Amplifier

Amirhossein Mohammadian[1], Abbas Mohammadi[1], Senior Member, IEEE, and
Abdolali Abdipour[1], Senior Member, IEEE, Mina Baghani[1]

Abstract

General frequency division multiplexing (GFDM) is a flexible non-orthogonal waveform candidate for 5G which can offer some advantages such as low out-of-band (OOB) emission and high spectral efficiency. In this paper, the effects of nonlinear behavior of practical PAs on GFDM signal are studied. In the first step, a closed form expression for power spectral density (PSD) of GFDM signal is extracted. Then, the PSD at the output of PA as a function of input power and the coefficients of nonlinear polynomial PA model is derived. In addition, the adjacent channel power (ACP) and ACP ratio, as two important performance metrics, are evaluated. The simulation results confirm the accuracy of derived analytical expressions. Moreover, to validate the performance of GFDM modulation after nonlinear PA, it is compared with OFDM modulation.

Index Terms

5G, GFDM modulation, Power amplifier nonlinearity, Power spectral density, Adjacent channel interference, Saturation and 1dB compression points

I. INTRODUCTION

Wide range of applications such as internet of things (IoT), machine-to-machine (M2M) communication, vehicle-to-vehicle (V2V) communication, tactile internet and cognitive radio are turning points in emergence of next generation wireless cellular networks (5G) [1]. For accomplishing these applications implementation, the next generation of the wireless systems

[1] Microwave / Millimeter-Wave and Wireless Communications Research Lab., Electrical Engineering Department, Amirkabir University of Technology, Tehran, Iran (e-mail: amirmohammadian, abm125, abdipour, baghani@aut.ac.ir).

must overcome the challenges such as lower power consumption, higher spectral efficiency, lower out-of-band emission and lower latency compared to the previous generation of wireless communication systems [1], [2]. Indispensable role of modulation technique in addressing these requirements is undeniable.

Orthogonal frequency division multiplexing (OFDM) scheme is a common multi-carrier modulation which is used in physical layer of the modern cellular communication system [3]. In spite of its simple implementation [4], it cannot deal with all vital requirements of 5G. Solid synchronization requirement in order to keep the orthogonality of OFDM subcarriers impose higher power consumption [1]. Moreover, by adding cyclic prefix to each OFDM symbol, obtaining high throughput is not easily achievable [5]. In addition, high out-of-band (OOB) emission of OFDM [6] is absolutely inefficient for cognitive radio networks and multiple access scenarios. Thus, the limitations of OFDM modulation in satisfying these requirements forces next generation networks to use a new modulation technique [1]. Filter bank multicarrier (FBMC) [7] and generalized frequency division multiplexing (GFDM) [8] are two potential candidates of non-orthogonal waveform for 5G networks. Even though, FBMC has ultra low OOB and high spectral efficiency, it has some drawbacks including difficulty of equalization process for frequency selective fading channel and its complexity for MIMO implementation [9], [10]. Hence, we consider GFDM waveform in this paper.

GFDM is a flexible non-orthogonal multi-carrier modulation which is proposed in [8]. As a block-based modulation scheme, GFDM includes number of subcarriers, each one carries subsymbols generated in multiple time slots. The subcarriers are individually pulse-shaped with a prototype filter using circular convolution. Flexibility of GFDM pertains to degrees of freedom measured by prototype filter and number of subcarriers and subsymbols. As a consequence of selecting pulse shaping filter, OOB emissions of GFDM degrades and therefore makes it attractive for noncontiguous frequency bands. In addition, the synchronization requirements of GFDM could be relaxed by utilizing additional cyclic suffix [8]. Moreover, by adding cyclic prefix to the entire block instead of each timeslot, higher spectral efficiency is achieved in compare with OFDM modulation.

GFDM modulation as a multicarrier modulation based on filter bank concept was initially discussed in [11]. The matrix model of GFDM transmitter was derived in linear form in [12]. Moreover, by using different prototype filters, the BER and OOB emission of GFDM were

studied and the effectiveness of pulse shaping on GFDM performance was studied in [13]. The adaptation of GFDM to 5G applications was shown in [8] by analyzing many characteristics of it. Although GFDM is a promising candidate for 5G, its practical implementation is confined with some impairments. One of them is high complexity compared to OFDM which is a major disadvantage. Accordingly, the complexity in the receiver was reduced by representing GFDM in frequency domain and employing sparse feature of filter in [14]. Also, a modem structure with low computational cost based on fast Fourier transform (FFT) was recently presented in [15]. Nonlinear nature of power amplifier (PA) is another practical impairment which may influence the GFDM performance.

PA is one of the most important elements of radio frequency (RF) chain in all wireless communication systems [16]. The PA linearity and efficiency are two conflicting but important factors. In other words, by moving the operating point towards the saturation point, PA efficiency increases while its linearity decreases [17]. According to increase in power consumption of communication systems in which PA has a huge part, utilizing the PA in high efficiency region is necessitated. Therefore, investigating the influence of PA's nonlinear behavior on system's performances is pivotal. Due to the nonlinear behavior of PA, AM/AM and AM/PM distortions may occur [18]. These destructive effects should be investigated for different types of input signal including GFDM. The authors in [19] has designed a receiver which estimates noise generated by in-band distortion of nonlinear PA and compensates its effects. In addition to in-band distortion, nonlinear nature of PA causes out-of-band distortion but to the best of our knowledge, none of the articles has investigated the GFDM out-of-band spectrum expansion, called spectral regrowth [20]. This issue is critical in multiple access scenarios and specially cognitive radio networks in which unlicensed users are not allowed to produce interference on the active licensed users on the adjacent channels [21]. This motivates us to investigate the power leakage of GFDM on the adjacent channels due to the nonlinear PA.

Many articles have focused on the effects of nonlinear behavior of PA for both single carrier and multicarrier input signals. The spectral regrowth of stationary complex Gaussian input signal was derived by calculating the autocorrelation function of PA output signal [22]–[26]. Indeed, code devision multiple access (CDMA) in [22], [25], and OFDM in [23], [26] satisfied the conditions of input complex Gaussian distribution according to the central limit theorem for high number of users and subcarriers, respectively. Without considering Gaussian distribution for PA
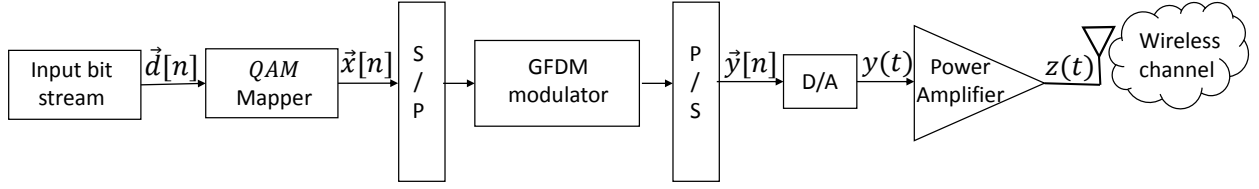
Fig. 1: Block diagram of transmitter

input signal, the autocovariance function of PA output was derived in [27]. In fact, assuming PA input to be a stationary process is not valid in most cases. Accordingly, the PSD expression of PA output was precisely derived for cyclostationary signals in [28]. More generally, by assuming orthogonality between subcarriers and time-limited pulse shape, a mathematical model of PSD for multi-carrier signals was derived in [29] which by considering its assumptions, the method can not be applied to GFDM. Finally, these analysis should be considered in system design especially in cognitive radio network. Thus, the results of nonlinearity analysis in single carrier and multicarrier were used in [30] and [31] for resource allocation in cognitive radio network, respectively.

In this paper, the PA nonlinearity distortion on the GFDM modulated signal is analyzed. For this purpose, the closed-form expressions for PSD of GFDM signal is derived. In the following, we assume that the nonlinear behavior of PA is modeled by polynomial function. Then, the PSD of nonlinear PA output signal is analyzed. Accordingly, closed-form expression of two critical points known as 1dB compression and saturation points are calculated. Moreover, the adjacent channel power (ACP) and the adjacent channel power ratio (ACPR) metrics which show basic information about power leakage in the adjacent channel are considered. Finally, to indicate the performance of GFDM after passing through nonlinear PA, it is compared with OFDM.

The rest of this paper is organized as follows: a system model is presented in Section II. The PSD and autocorrelation function of GFDM signal and PA output are calculated in Section III. The ACP and ACPR, 1dB compression and saturation points are derived in Section IV. The accuracy of analytical expressions are examined in Section V by means of simulation results. Finally, conclusion remarks are provided in Section VI.
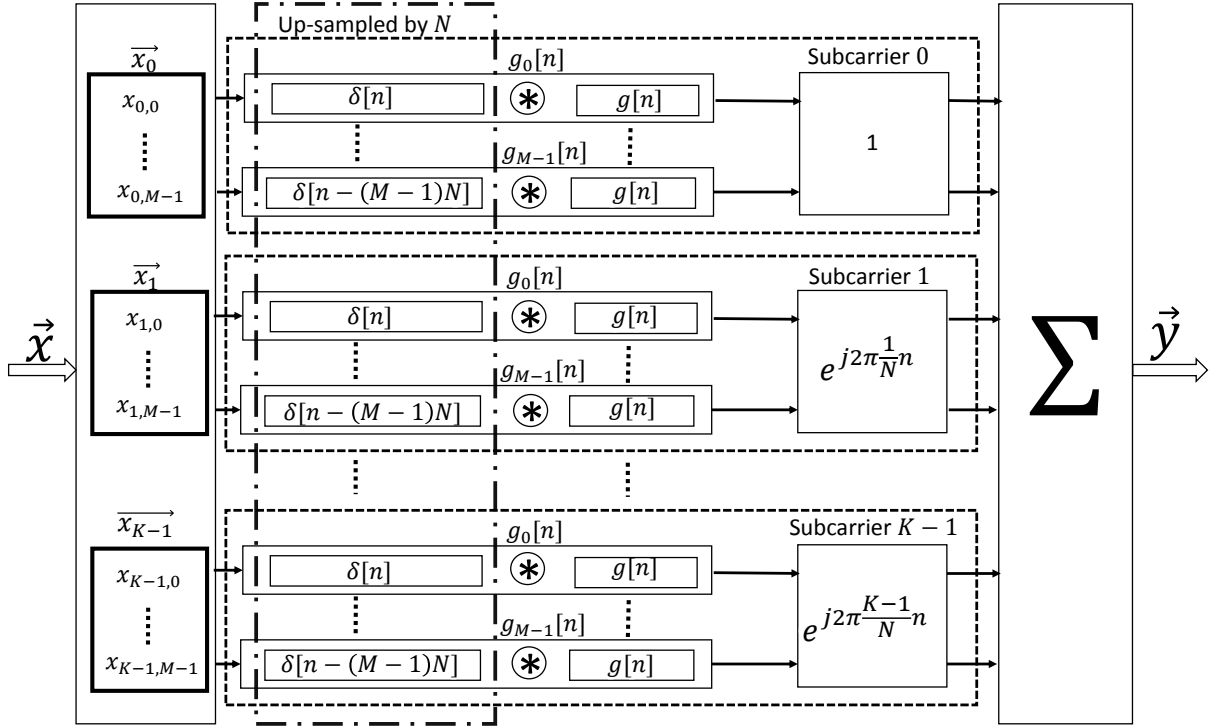
Fig. 2: GFDM modulator structure

II. SYSTEM MODEL

The block diagram of typical transmitter is illustrated in Fig. 1, which contains GFDM modulator. In the first step, to generate symbols, input bit stream, $\vec{d}$, is fed into mapper, e.g. QAM with modulation order of μ. Then, vector $\vec{x}$, is converted from serial to parallel form and is passed through the GFDM modulator. Finally, the resulting vector $\vec{y}$, converted from parallel to serial, is amplified by PA. In the next two subsections, we explain GFDM modulator and PA structures.

A. GFDM modulator structure

The GFDM modulator structure is shown in Fig. 2 where M subsymbols per block are transmitted on K subcarriers. The input of GFDM modulator is vector $\vec{x}$, contains of MK complex data symbols, which are independent and identically distributed ($i.i.d$). Symbols of block can be formed as $\vec{x} = [[x_0]^T, [x_1]^T, [x_2]^T, ..., [x_{K-1}]^T]^T$, including K vectors each has M elements, $[x_k] = [x_{k,0}, x_{k,1}, x_{k,2}, ..., x_{k,M-1}]^T$. $x_{k,m}$ is indicator of mth transmitted subsymbol

on the kth subcarrier, $k = 0, 1, ..., K - 1$ and $m = 0, 1, ..., M - 1$. According to Fig. 2, data symbols are up-sampled by the factor of N where N is the number of samples per symbol. Resulting vector is in the form of

$$s_k[n] = \sqrt{\alpha} \sum_{m=0}^{M-1} x_{k,m} \delta[n - mN] \tag{1}$$

where α is power scaling factor. Vector $s_k = [s_k[0], s_k[1], s_k[2], ..., s_k[MN - 1]]$ is circularly convolved with vector $\vec{g}$, which holds all coefficients of the prototype filter with the length MN. Finally, after up-converting to the frequency of intended subcarrier, the resulting signals are summed. Due to the circular convolution characteristics, the output of GFDM modulator per frame can be written as [15]

$$
\begin{aligned}
y_v[n] &= \sqrt{\alpha} \sum_{k=0}^{K-1} (s_k[n] \circledast g[n]) e^{j2\pi \frac{(k - \frac{K-1}{2})}{N} n} \\
&= \sqrt{\alpha} \sum_{k=0}^{K-1} \sum_{m=0}^{M-1} x_{k,m} g[n - mN]_{MN} e^{j2\pi \frac{(k - \frac{K-1}{2})}{N} n} \qquad 0 \leq n \leq MN - 1
\end{aligned} \tag{2}
$$

where v is the frame index and $\circledast$ denotes the circular convolution. By concatenating blocks, the GFDM signal can be expressed as

$$y[n] = \sqrt{\alpha} \sum_{v=-\infty}^{\infty} \sum_{k=0}^{K-1} \sum_{m=0}^{M-1} x_{k,m,v} g_m[n - vMN] \, e^{j2\pi \frac{(k - \frac{K-1}{2})}{N} n} \qquad -\infty \leq n \leq \infty \tag{3}$$

where $g_m[n] = g[n - mN]_{MN}$ is circularly shifted version of $g[n]$.

The continuous-time version of the GFDM modulation signal can be written as

$$y(t) = \sqrt{\alpha} \sum_{v=-\infty}^{\infty} \sum_{k=0}^{K-1} \sum_{m=0}^{M-1} x_{k,m,v} g_m(t - vT_B) \, e^{j2\pi \frac{(k - \frac{K-1}{2})}{T_s} t} \qquad -\infty \leq t \leq \infty \tag{4}$$

where T_s is the symbol duration, $g_m(t)$ is continuous form of $g_m[n]$ with the length of MT_s and T_B is block duration which is equal to MT_s, respectively. By considering $\frac{N}{T_s}$ as sampling

frequency, MN discrete samples in (2) are obtained. Since $\frac{1}{T_s}$ is bandwidth allocated to each subcarrier, the total bandwidth is $\frac{K}{T_s}$ by considering K subcarriers.

B. Power amplifier

In this paper, to investigate the performance of nonlinear PA, behavioral modeling techniques are considered. A popular technique to model the nonlinearity of narrowband and memory less PA is polynomial function as follows as [20]

$$z(t) = \sum_{i=0}^{2N_p+1} a_{2i+1}|y(t)|^{2i}y(t) \tag{5}$$

where $z(t)$ is corresponding output of PA, a_{2i+1} are complex coefficients, $y(t)$ is the baseband input signal and $2N_p+1$ is the order of nonlinearity. In-band and adjacent-band intermodulation distortions are caused only by odd terms of nonlinearity [22], which can be determined by single-tone complex compression characteristics [32].

III. POWER SPECTRAL DENSITY

Nonlinear nature of PA causes out-of-band distortion. By using the polynomial modeling of PA in time domain, convolution terms appear in frequency response which result in spectral regrowth. As it is shown in Fig. 3, by considering nonlinear PA model, the spectrum of its output signal is expanded. To investigate the effect of PA nonlinearity on OOB leakage, the spectrum of PA output signal should be calculated. Since the spectrum of output signal is undoubtedly a function of input signal, PSD of GFDM signal, as PA input, should be derived. Accordingly , in this section, PSD of GFDM is extracted and then, PSD of PA output is obtained

A. PSD of GFDM modulated signal

In order to calculate the PSD of GFDM modulated signal, autocorrelation function of transmitted baseband GFDM signal, $y(t)$, should be derived. By using (4), the autocorrelation function is written as follows
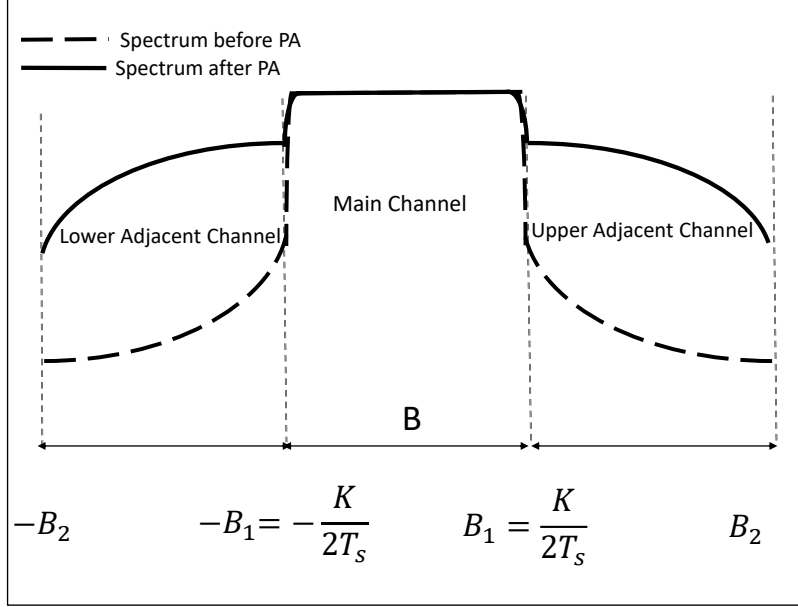
Fig. 3: The normalized PSD of the input and output nonlinear PA

$$R_{yy}(t,\tau) = E[y(t)y^*(t-\tau)]$$

$$= \alpha \sum_{\upsilon_1=-\infty}^{\infty} \sum_{\upsilon_2=-\infty}^{\infty} \sum_{k_1=0}^{K-1} \sum_{k_2=0}^{K-1} \sum_{m_1=0}^{M-1} \sum_{m_2=0}^{M-1} E[x_{k_1,m_1,\upsilon_1} x^*_{k_2,m_2,\upsilon_2}] g_{m_1}(t-\upsilon_1 T_B) g^*_{m_2}(t-\tau-\upsilon_2 T_B)$$

$$\times e^{j2\pi \frac{(k_1 - \frac{K-1}{2})}{T_s} t} e^{-j2\pi \frac{(k_2 - \frac{K-1}{2})}{T_s}(t-\tau)}$$

$$(6)$$

where data symbol $x_{k,m,\upsilon}$ is independent and identically distributed random variable. Thus, autocorrelation function of $x_{k,m,\upsilon}$ can be shown as

$$E[x_{k_1,m_1,\upsilon_1} x^*_{k_2,m_2,\upsilon_2}] = \overline{p}_x \delta(k_1 - k_2)\delta(m_1 - m_2)\delta(\upsilon_1 - \upsilon_2) \tag{7}$$

where $\overline{p}_x$ is the average power of data symbols. In this paper, QAM modulation of order μ is considered which its average power is equal to $\overline{P_x} = \frac{2((2^\mu)-1)}{3}$ [33]. By considering (7), the equation (6) has nonzero value for $k_1 = k_2 = k$, $m_1 = m_2 = m$ and $\upsilon_1 = \upsilon_2 = \upsilon$, thus

$$R_{yy}(t,\tau) = \alpha \overline{p}_x \sum_{v=-\infty}^{\infty} \sum_{k=0}^{K-1} \sum_{m=0}^{M-1} g_m(t - vT_B)g_m^*(t - \tau - vT_B)e^{j2\pi \frac{(k - \frac{K-1}{2})}{T_s}\tau}. \qquad (8)$$

According to (8), autocorrelation function is time dependent and the signal is not stationary. However, $R_{yy}(t,\tau)$ is periodic by $T_B = MT_s$, which means that $y(t)$ is cyclostationary with period MT_s. Time dependency of $R_{yy}(t,\tau)$ can be omitted by calculating average of autocorrelation function over a period as follows

$$\overline{R}_{yy}(\tau) = \frac{\alpha \overline{p}_x}{MT_s} \int_0^{MT_s} \sum_{v=-\infty}^{\infty} \sum_{k=0}^{K-1} \sum_{m=0}^{M-1} g_m(t - vT_B)g_m^*(t - \tau - vT_B)e^{j2\pi \frac{(k - \frac{K-1}{2})}{T_s}\tau} dt$$

$$= \frac{\alpha \overline{p}_x}{MT_s} \overline{R}_{GG}(\tau) \sum_{k=0}^{K-1} e^{j2\pi \frac{(k - \frac{K-1}{2})}{T_s}\tau}. \qquad (9)$$

By using linear convolution formula and considering $g_m(t)$ as a real term , $\overline{R}_{GG}(\tau)$ can be found as

$$\overline{R}_{GG}(\tau) = \int_0^{MT_s} \sum_{v=-\infty}^{\infty} \sum_{m=0}^{M-1} g_m(t - vT_B)g_m^*(t - \tau - vT_B)dt$$

$$= \sum_{m=0}^{M-1} \int_{-\infty}^{\infty} g_m(t)g_m^*(t - \tau)dt = \sum_{m=0}^{M-1} g_m(\tau) \otimes g_m(-\tau) \qquad (10)$$

where $\otimes$ denotes the linear convolution. By taking FT (Fourier Transform) of $\bar{R}_{yy}(\tau)$ to obtain the PSD of $y(t)$, we have

$$S_{yy}(f) = \int_{-\infty}^{\infty} \overline{R}_{yy}(\tau)e^{-j2\pi f\tau}d\tau = \frac{\alpha \overline{p}_x}{MT_s} \sum_{k=0}^{K-1} \int_{-\infty}^{\infty} \overline{R}_{GG}(\tau)e^{-j2\pi(f - \frac{(k - \frac{K-1}{2})}{T_s})\tau}d\tau$$

$$= \frac{\alpha \overline{p}_x}{MT_s} \sum_{k=0}^{K-1} S_{GG}(f - \frac{(k - \frac{K-1}{2})}{T_s}) \qquad (11)$$

where $S_{GG}(f)$ is

$$
\begin{aligned}
S_{GG}(f) &= \int\limits_{-\infty}^{\infty} \overline{R}_{GG}(\tau)e^{-j2\pi f\tau}d\tau = \int\limits_{-\infty}^{\infty} \sum_{m=0}^{M-1} (g_m(\tau) \otimes g_m(-\tau))e^{-j2\pi f\tau}d\tau \\
&= \sum_{m=0}^{M-1} \int\limits_{-\infty}^{\infty} (g_m(\tau) \otimes g_m(-\tau))e^{-j2\pi f\tau}d\tau = \sum_{m=0}^{M-1} G_m(f)G_m^*(-f) = \sum_{m=0}^{M-1} |G_m(f)|^2.
\end{aligned}
\tag{12}
$$

By confining signal in time, frequency expansion occurs. Even though, a pulse shaped filter such as raised cosine is used, the limited power leaks into adjacent bands. In order to estimate amount of energy emission in out-of-band frequency interval, OOB as a ratio between the amount of energy in out-of-band (OB) and in-band (IB) frequency range is defined as [8]

$$
OOB = \frac{|IB|}{|OB|} \cdot \frac{\int\limits_{f \in OB} S_{yy}(f)df}{\int\limits_{f \in IB} S_{yy}(f)df}.
\tag{13}
$$

B. PSD of PA output signal

PSD of PA output can be calculated by finding its autocorrelation function. According to (5), the autocorrelation function of PA output is as follows

$$
\begin{aligned}
R_{zz}(t,\tau) &= E[z(t)z^*(t-\tau)] = E\Big[\sum_{i_1=0}^{2N_p+1} a_{2i_1+1}|y(t)|^{2i_1}y(t) \times \sum_{i_2=0}^{2N_p+1} a_{2i_2+1}^*|y(t-\tau)|^{2i_2}y^*(t-\tau)\Big] \\
&= \sum_{i_1=0}^{2N_p+1} \sum_{i_2=0}^{2N_p+1} a_{2i_1+1}a_{2i_2+1}^*\phi_{i_1,i_2}(t,\tau)
\end{aligned}
\tag{14}
$$

where $\phi_{i_1,i_2}(t,\tau) = E[y(t)^{i_1+1}y(t-\tau)^{i_2}(y^*(t))^{i_1}(y^*(t-\tau))^{i_2+1}]$.

By considering (3) and (4), $y(t)$ is continuous time version of $y[n]$ which is derived from summation of MN independent, identically distributed random variables. Due to central limit theorem [33] as MN gets large, the distributions of $y(t)$ becomes Gaussian. By utilizing moments of complex Gaussian random variable $y(t)$, $\phi_{i_1,i_2}(t,\tau)$ can be derived as

$$
\begin{aligned}
\phi_{i_1,i_2}(t,\tau) &= \sum_{p=0}^{\min(i_1,i_2)} \binom{i_2+1}{p+1}\binom{i_1+1}{p+1}\binom{i_2}{p}\binom{i_1}{p}(p+1)!(p)!(i_2-p)!(i_1-p)! \\
&\quad (R_{yy}(t,\tau))^{p+1}(R_{yy}^*(t,\tau))^p(R_{yy}(t,0))^{i_1+i_2-2p}
\end{aligned}
\tag{15}
$$

where, $\begin{pmatrix} i \\ p \end{pmatrix} = \frac{i!}{p!i-p!}$. The detail of (15) is expressed in Appendix A. Based on (8), (14) and

(15), the autocorrelation function of PA output, $R_{zz}(t,\tau)$, can be derived.

Due to the fact that $R_{yy}(t,\tau) = R_{yy}(t+MT_s,\tau)$, $\phi_{i_1,i_2}(t,\tau)$ is periodic by MT_s in (15). Thus, in (14), it is clear that $R_{zz}(t,\tau) = R_{zz}(t+MT_s,\tau)$, which shows that $z(t)$ is cyclostationary. Thus, by using (14), the average of PA output autocorrelation function can be calculated as

$$
\overline{R}_{zz}(\tau) = \frac{1}{MT_s} \int_0^{MT_s} R_{zz}(t,\tau)dt = \frac{1}{MT_s} \int_0^{MT_s} \sum_{i_1=0}^{2N_p+1} \sum_{i_2=0}^{2N_p+1} a_{2i_1+1} a_{2i_2+1}^* \phi_{i_1,i_2}(t,\tau)dt
$$

$$
= \sum_{i_1=0}^{2N_p+1} \sum_{i_2=0}^{2N_p+1} a_{2i_1+1} a_{2i_2+1}^* \phi_{i_1,i_2}(\tau)
$$

(16)

where $\phi_{i_1,i_2}(\tau) = \frac{1}{MT_s} \int_0^{MT_s} \phi_{i_1,i_2}(t,\tau)dt$. Finally, by taking FT (Fourier Transform) of (16), the PSD of $z(t)$ can be calculated as

$$
S_{zz}(f) = \int_{-\infty}^{\infty} \overline{R}_{zz}(\tau)e^{-j2\pi f\tau}d\tau = \int_{-\infty}^{\infty} \sum_{i_1=0}^{2N_p+1} \sum_{i_2=0}^{2N_p+1} a_{2i_1+1} a_{2i_2+1}^* \phi_{i_1,i_2}(\tau)e^{-j2\pi f\tau}d\tau
$$

$$
= \sum_{i_1=0}^{2N_p+1} \sum_{i_2=0}^{2N_p+1} a_{2i_1+1} a_{2i_2+1}^* \phi_{i_1,i_2}(f).
$$

(17)

By considering $\phi_{i_1,i_2}(f) = \int_{-\infty}^{\infty} \phi_{i_1,i_2}(\tau)e^{-j2\pi f\tau}d\tau$, the PSD of PA output is derived as

$$
S_{zz}(f) = \sum_{i_1=0}^{2N_p+1} \sum_{i_2=0}^{2N_p+1} a_{2i_1+1} a_{2i_2+1}^*
$$

$$
\sum_{p=0}^{\min(i_1,i_2)} \begin{pmatrix} i_2+1 \\ p+1 \end{pmatrix} \begin{pmatrix} i_1+1 \\ p+1 \end{pmatrix} \begin{pmatrix} i_2 \\ p \end{pmatrix} \begin{pmatrix} i_1 \\ p \end{pmatrix} (p+1)!(p)!(i_2-p)!(i_1-p)!(\alpha\overline{p}_x)^{i_1+i_2+1}(K)^{i_1+i_2-2p} \frac{1}{MT_s}
$$

$$
P_{i_1,i_2}(f) \otimes \left(\sum_{k_1,\ldots,k_{p+1}=0}^{K-1} \sum_{k_1',\ldots,k_p'=0}^{K-1} \delta(f - \frac{(\sum_{j=1}^{p+1} k_j - \sum_{j'=1}^{p} k_{j'} - \frac{K-1}{2})}{T_s}) \right)
$$

(18)

where $P_{i_1,i_2}(f)$ is equal to

$$P_{i_1,i_2}(f) = \sum_{m_1,\dots,m_{p+1}=0}^{M-1} \sum_{m_1',\dots,m_p'=0}^{M-1} \sum_{m_1'',\dots,m_{i_1+i_2-2p}''=0}^{M-1} \Big(G_{m_1}(f),\dots \otimes G_{m_{p+1}}(f) \otimes G_{m_1'}^*(-f)$$

$$\otimes\ G_{m_p'}^*(-f) \otimes G_{m_1''}^*(-f) \otimes \dots \otimes G_{m_{i_1+i_2-2p}''}^*(-f) \otimes G_{m_1''}(f) \otimes \dots \otimes G_{m_{i_1+i_2-2p}''}(f) \Big)$$

$$\times \Big(G_{m_1}^*(f) \otimes \dots \otimes G_{m_{p+1}}^*(f) \otimes G_{m_1'}(-f) \otimes \dots \otimes G_{m_p'}(-f) \Big)$$

$$\tag{19}$$

The detail of (18) and (19) is expressed in Appendix B. As it is clear from (19), $P_{i_1,i_2}(f)$ only depends on filters which are extracted from prototype filter. Indeed, (18) is a closed form generic function for PSD of PA output signal.

IV. NONLINEAR PARAMETER EXTRACTION

A suitable operating point of a nonlinear PA can be selected by considering 1dB compression point and saturation point. The point in which the output power of a nonlinear PA is 1dB below the linear one, is known as 1dB compression point. Also, saturation point specifies the saturation region of PA where increase in input power causes no further rise in output power. On the other hand, due to nonlinear behavior of PA, the spectrum of transmitted signal can leak into adjacent frequency bands. By calculating ACP, this disruptive effect caused by nonlinear PA can be predicted for any input power scaling factor. The ratio between ACP and the power in the main channel is called ACPR. In this section, first, a closed-form expression of 1dB compression point and saturation point are derived. Then, ACP and ACP metrics are considered.

A. 1dB compression point and saturation point

In order to calculate the 1dB compression point, the total nonlinear PA output power should be obtained as a function of input power scaling factor. According to (16), the total output power can be expressed as

$$P_z(\alpha) = \overline{R}_{zz}(0) = \sum_{i_1=0}^{2N_p+1} \sum_{i_2=0}^{2N_p+1} a_{2i_1+1} a^*_{2i_2+1} \phi_{i_1,i_2}(0) \tag{20}$$

where

$$\phi_{i_1,i_2}(0) = \frac{1}{MT_s} \sum_{p=0}^{\min(i_1,i_2)} \binom{i_2+1}{p+1}\binom{i_1+1}{p+1}\binom{i_2}{p}\binom{i_1}{p}(p+1)!(p)!(i_2-p)!(i_1-p)!$$

$$\int_0^{MT_s} (R_{yy}(t,0))^{i_1+i_2+1} dt. \tag{21}$$

Note that $R_{yy}(t,0) = \alpha K \overline{p}_x \sum_{m=0}^{M-1} |g_m(t)|^2$. According to (8), $R_{yy}(t,0)$ is function of α, thus the total output power as a function of input power scaling factor can be expressed as

$$P_z(\alpha) = \sum_{j=1}^{\infty} A_j \alpha^j \tag{22}$$

where

$$A_j = \frac{(K\overline{p}_x)^j}{MT_s} \int_0^{MT_s} \left(\sum_{m=0}^{M-1} |g_m(t)|^2 \right)^j dt$$

$$\times \sum_{\substack{i_1+i_2+1=j \\ i_1+i_2 \geq 0}} a_{2i_1+1} a_{2i_2+1}^* \sum_{p=0}^{\min(i_1,i_2)} \binom{i_2+1}{p+1}\binom{i_1+1}{p+1}\binom{i_2}{p}\binom{i_1}{p}(p+1)!(p)!(i_2-p)!(i_1-p)!. \tag{23}$$

The saturation point is the smallest positive root of derivative of $P_z(\alpha)$ with respect to α which is derived as $\frac{\partial}{\partial z} P_z = \sum_{j=1}^{\infty} j A_j \alpha^{j-1} = 0$. Similarly, $1dB$ compression point is the smallest positive root of $10\log_{10}(P_z(\alpha)) = 10\log_{10}(A_1\alpha) - 1$ according to definition on it.

B. ACP and ACPR

As mentioned, ACP determines the amount of power in adjacent channel. By considering (18), PSD of PA output signal is obtained by summation of some terms which not only have the same bandwidth as GFDM signal $(-B_1 \leq f \leq B_1)$, but also have multiples of bandwidth of the main channel, which causes spectral regrowth. Therefore, the bandwidth of PA output signal is more than the input signal bandwidth. As a result, the ACP can be derived by integrating over the bandwidth of upper or lower adjacent channel. In general, upper ACP can be obtained by

TABLE I: Parameters of GFDM modulation and Nonlinear coefficients of the PA model.

Parameter	Value
Mapping	$16 - QAM$
Filter type	$Raised - cosine$
Roll-off factor	0.3
Symbol duration (T_s)	33.3 μs
Number of subcarrier (K)	64
Samples per symbol (N)	320
Number of subsymbols (M)	5 and 35
Subcarrier spacing ($\frac{1}{T_s}$)	30 kHz
Signal Bandwidth ($2B_1 = \frac{K}{T_s}$)	1.92 MHz
Sampling frequency ($\frac{N}{T_s}$)	9.6 MHz
Nonlinear coefficient (a_1)	14.9740 +j0.0519
Nonlinear coefficient (a_3)	-23.0954 +j4.9680
Nonlinear coefficient (a_5)	21.3936 +j0.4305

$$ACP(p) = \int\limits_{B_1}^{B_2} S_{zz}(f)df. \tag{24}$$

As can be seen in Fig. 3 , $[B_1, B_2]$ is a frequency interval of upper adjacent channel. Moreover, ratio between power of adjacent channel to the power of main channel, ACPR, is expressed as

$$ACPR(p) = \frac{ACP(p)}{\int\limits_{-B_1}^{B_1} S_{zz}(f)df} \tag{25}$$

where $[-B_1, B_1]$ is a frequency interval of the main channel.

V. SIMULATION AND NUMERICAL RESULTS

In this section, derived analytical expressions are verified with simulation results. Parameters of GFDM modulation and complex coefficients of a fifth order polynomial function of PA model [34] are represented in table I. Monte Carlo simulation with 1000 GFDM symbols is used to generate GFDM modulated signal. To estimate the PSD, averaged periodogram algorithm with 50% overlap and hanning window is used [35]. For extracting simulation results, the length of FFT is set to 65536. Causal and FIR prototype filter, $g(t)$, is shifted length $\frac{MT_s}{2}$ of truncated
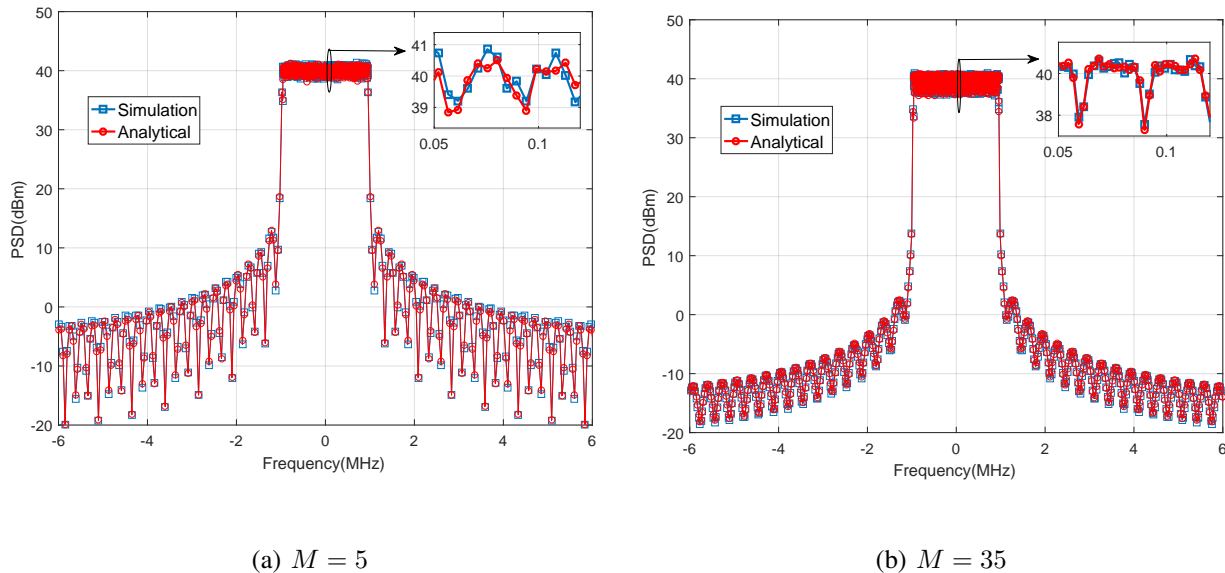
(a) $M = 5$ (b) $M = 35$

Fig. 4: Power spectral density of GFDM modulated signal for two different of subsymbols.

infinite Raised cosine filter in interval $\left[\frac{-MT_s}{2}, \frac{MT_s}{2}\right]$ which is normalized to unit energy. According to $g(t)$, other filters, $g_m(t)$, are as follows

$$g_m(t) = \begin{cases} g(t - mT_s), \ mT_s < t \le MT_s \\ g((M - m)T_s + t), \ 0 < t \le mT_s \end{cases} \tag{26}$$

Furthermore, $g_m[n]$ are filter coefficients which are discrete form of $g_m(t)$. To evaluate nonlinear behavior of PA, the PSD of PA output should be calculated. For this purpose, PSD of GFDM signal is simulated for given parameters. Then, by simulating PSD of PA output, its spectrum expansion is studied . Note that all simulation results are verified with analytic expression.

A. PSD of GFDM signal

In this part, PSD of GFDM signal are examined and the parameters which have effect on it, are investigated. In Fig. 4, PSDs of GFDM modulated signals with $k = 64$ (number of subcarriers) and two different numbers of subsymbols ($M = 5$ and $M = 35$) are illustrated, where the scaling factor, $p = 1$, is considered in these two figures. As can be seen, the simulation results verify the derived analytical formula for PSD of GFDM (11). By comparing Fig. 4(a) and Fig. 4(b), it can be concluded that difference between in-band and out-of-band values of PSD is varied
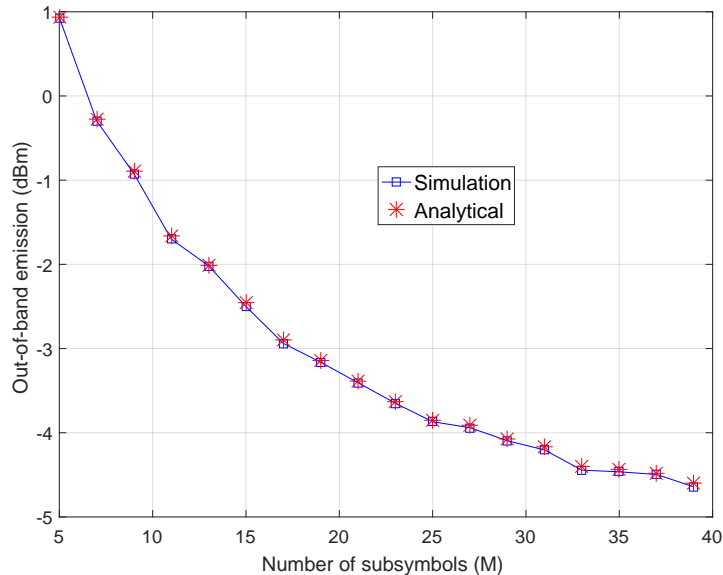
Fig. 5: OOB radiation of GFDM versus different numbers of subsymbols

for different number of subsymbols. OOB radiation for $M = 35$ is approximately $6dB$ below for $M = 5$. To justify this behavior, we refer to the procedure of truncating infinite filter for obtaining prototype filter which causes appearance of nonzero side lobes in frequency domain. By increasing the number of subsymbols, time span of filter increases and the spectrum approaches to its ideal position which causes suppression of side lobs. Consequently, by increasing the number of time slots, OOB leakage of GFDM signal which is a result of side lobe reduction, is diminished.

In Fig. 5, OOB leakages of GFDM modulated signal with 64 subcarriers versus varied number of subsymbols is represented in which the input power scaling factor is same as Fig(4). In both simulation and analytic result (13), frequency of OOB and B is considered in the range of $[0.96, 4.8]_{MHz}$ and $[-0.96, 0.96]_{MHz}$, respectively. As expected, increasing the number of subsymbols causes reduction in OOB leakage. However, the other performance metrics of system, such as bit error rate, may be degraded. Again, the simulation result verifies the derived analytical formula.
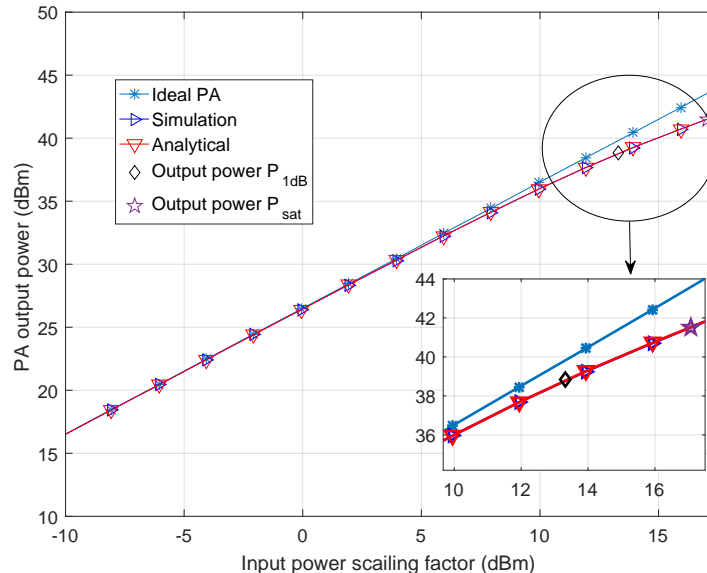
Fig. 6: PA output power curves versus input power scaling factor.

B. PSD of output PA

In pervious part, PSD of GFDM signal is investigated. In this part, the effects of PA non-linearity on GFDM signal performance will be considered. For this purpose, first the analytical expressions of PA output power, 1dB compression and saturation points as critical points of given PA model are verified by simulation result. After that, PSD of PA output and ACP/ACPR metrics, by given analytical formulas, are studied. Similarly, two sets of GFDM, 64 subcarriers and 5, 35 subsymbols, are considered to show the effect of different number of subsymbol on the results.

Fig. 6 represents AM/AM characteristic of considered PA model derived by simulation and analytical formula (22). Also, the 1dB compression and saturation points are $p_{1dB} = 13.3dBm$ and $p_{sat} = 17.07dBm$. This figure shows that theoretical and simulation results are clearly matched with each other so the total PA output power expression in (22) is verified.

In Fig. 7, PSD of PA output (equation (18)) is compared with the simulation results. In both Fig. 7(a) and Fig. 7(b), PSDs of output signal of power amplifier are depicted for three input power scaling factors $\alpha = 5dBm$, $\alpha = p_{1dB}$ and $\alpha = p_{sat}$. Note that the first one is selected in linear region of PA. As expected, by increasing the input power scaling factor and approaching to the saturation point, adjacent channel power in $[0.96, 4.8]_{MHz}$ interval increases. As it is shown
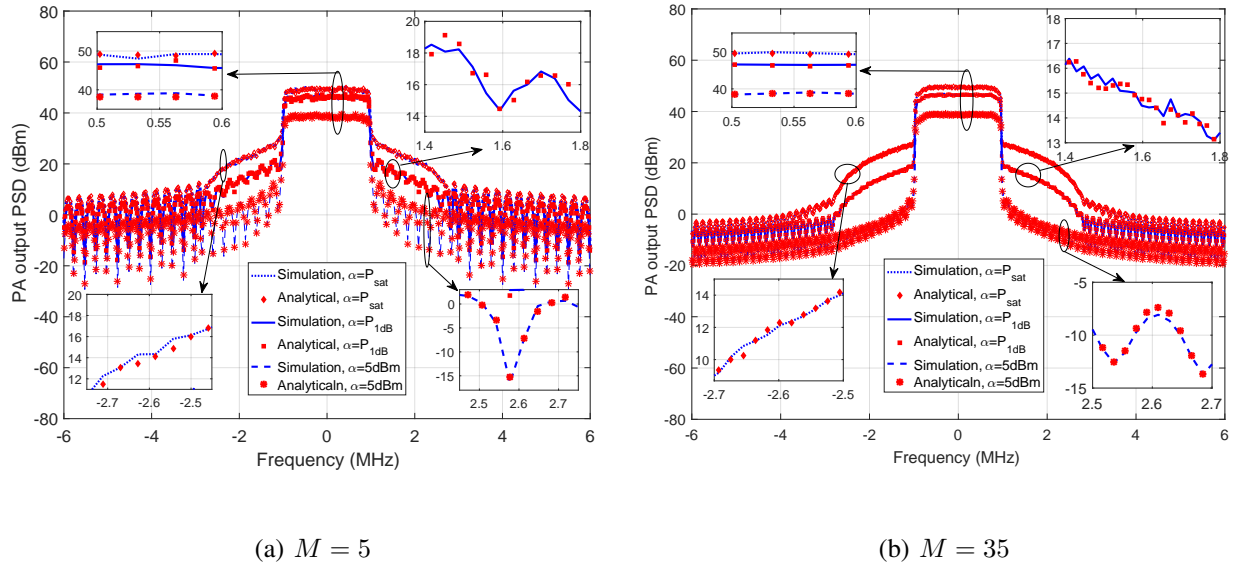
(a) $M = 5$

(b) $M = 35$

Fig. 7: Power spectral density of PA output for two diffrent number of subsymbols.
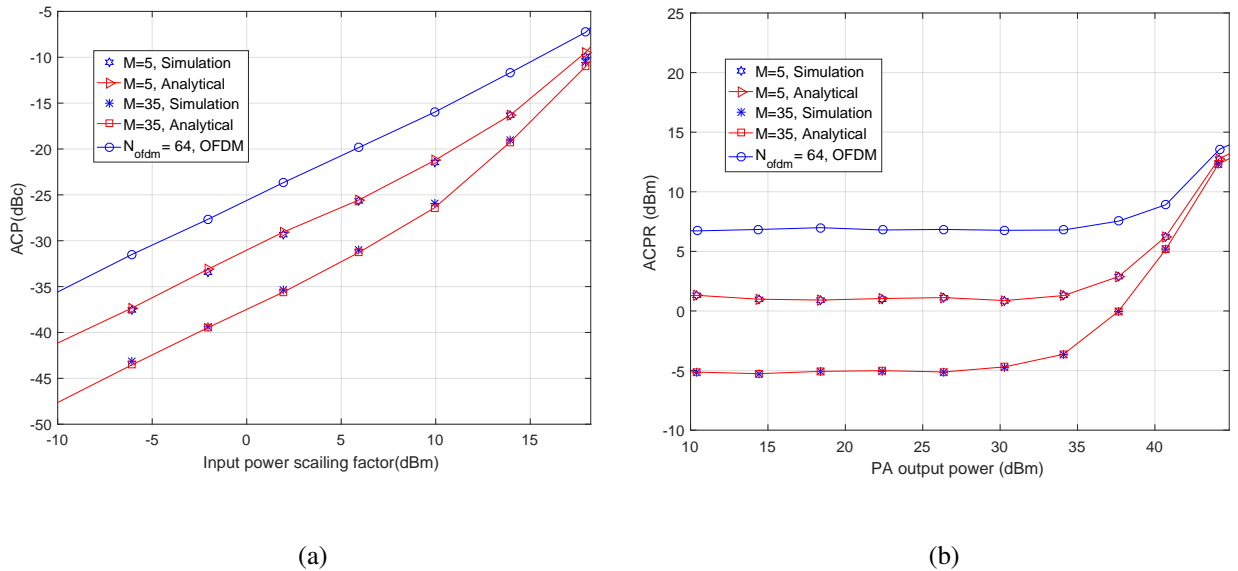

(a)

(b)

Fig. 8: (a) ACP versus input power scaling factor and (b) ACPR versus PA output power

in figures, by increasing the number of subsymbols, for two power inputs, p_{1dB} and p_{sat}, spectral regrowth approximately stays same and the number of subsymbols does not have effect on it. But, in $\alpha = 5dBm$, OOB radiation in adjacent channel for $M = 35$ is approximately $5dBm$ less than $M = 5$. It is due to the fact that by boosting the input power scaling factor, the impact of

the nonlinear terms in the spectral regrowth, which are produced by multiple self-convolution of GFDM spectrum, becomes stronger. Since the in-band spectrum of GFDM signal is independent of M, these terms are independent too. For $\alpha = 5dBm$, PA operates in linear region and PSD of its output is just relied on the linear term, though by increasing the number of subsymbols OOB leakage reduces. Therefore, by considering p_{1dB} and p_{sat} as input power scaling factors, the nonlinear terms have dominant influence and same result is obtained for $M = 5$ and $M = 35$ due to its independency of M.

In Fig. 8, simulation and analytical results of ACP and ACPR metrics are illustrated. As mentioned, $[0.96, 4.8]_{MHz}$ is considered as frequency interval of adjacent channel. In Fig. 8, theoretical expression of ACP in (24) and ACPR in (25) are compared with the Monte Carlo simulation results for two sets of GFDM modulations parameters to examine the accuracy of derived expressions. As expected, since PA operates in the linear region, OOB leakage is affected by number of subsymbols. By increasing the input power scaling factor and entering to the nonlinear region of PA, the spectral regrowth caused by nonlinearity is dominant and results in approaching to same value for $M = 5$ and $M = 35$. Moreover, ACP and ACPR of OFDM modulated signal with 64 subcarriers due to the nonlinear PA are represented in Fig. 8. As expected, GFDM modulated signal based on filter bank structure has better performance compared with OFDM modulated signal both in linear region and nonlinear region which shows that gain of GFDM modulated signal after PA is preserved.

VI. CONCLUSION

In this paper, by utilizing cyclostationary property of autocorrelation function of GFDM signal, the analytical expression of its PSD was derived. According to the derived analytical expression for PSD, OOB radiation of GFDM spectrum is decreased by increasing the number of subsymbols which is verified by simulation results. Then, by considering the polynomial function to model the nonlinear behavior of PA, the PSD of output signal was extracted and verified by simulation results. Amplitude (AM/AM) and Phase (AM/PM) distortions was considered with memoryless model. By representing PA output power as a function of input power and coefficients of polynomial function dependence of spectral regrowth to input power and the number of subsymbols was proved. For low input power, increasing the number of subsymbols causes reduction in OOB emission though, this effect is diminished for high input power by

approaching to nonlinear zone of PA. Moreover, ACP and ACPR were obtained which confirmed our aforementioned results. All analytical expressions were verified by simulation results by where a good agreement between them in all cases were obtained. Furthermore, comparison of PA output ACP and ACPR with OFDM input and GFDM input showed that the benefit of GFDM are preserved after PA.

APPENDIX A

Moments of complex Gaussian random variable l are given by [36]

$$
E[l_1 l_2 ..., l_s l_1^* l_2^* ...., l_m^*]
$$

$$
= \begin{cases} 0, s \neq m \\ \sum_{\pi} E[l_{\pi(1)} l_1^*] E[l_{\pi(2)} l_2^*], ..., E[l_{\pi(s)} l_m^*], s = m \end{cases} \tag{27}
$$

where $\{l_i, i = 1, 2, ...s, ..., m\}$ are complex Gaussian random variables and π is apermutation of the set of integers $\{1, 2, ..., s, ..., m\}$ [22]. Due to Gaussian distribution of $y(t)$, (27) is used to calculate $\phi_{i_1,i_2}(t, \tau) = E[y(t)^{i_1+1} y(t-\tau)^{i_2} (y^*(t))^{i_1} (y^*(t-\tau))^{i_2+1}]$ as

$$
\phi_{i_1,i_2}(t, \tau) = \sum_{\pi} E[y_{\pi(1)} y^*(t)], ..., E[y_{\pi(i_1)} y^*(t)] E[y_{\pi(i_1+1)} y^*(t-\tau)], ..., E[y_{\pi(i_1+i_2+1)} y^*(t-\tau)] \tag{28}
$$

where $s = m = i_1 + i_2 + 1$ and $y_i = \begin{cases} y(t) & i = 1, ..., i_1 + 1 \\ y(t-\tau) & i = i_1 + 2, ..., i_1 + i_2 + 1 \end{cases}$

By doing some manual calculation on (28), $\phi_{i_1,i_2}(t, \tau)$ is derived as

$$
\phi_{i_1,i_2}(t, \tau) = \sum_{p=0}^{\min(i_1,i_2)} \binom{i_2+1}{p+1} \binom{i_1+1}{p+1} \binom{i_2}{p} \binom{i_1}{p} (p+1)!(p)!(i_2-p)!(i_1-p)!
$$

$$
(R_{yy}(t, \tau))^{p+1} (R_{yy}^*(t, \tau))^p (R_{yy}(t, 0))^{i_1+i_2-2p} \tag{29}
$$

APPENDIX B

By considering (8), (15) and (16), $\phi_{i_1,i_2}(\tau)$ is derived. In the following, by taking FT of it, $\phi_{i_1,i_2}(f) = \int\limits_{-\infty}^{\infty} \phi_{i_1,i_2}(\tau) e^{-j2\pi f\tau} d\tau$ is calculated as

$$\phi_{i_1,i_2}(f) = \sum_{p=0}^{\min(i_1,i_2)} T_{i_1,i_2}$$

$$\times \left(\begin{array}{c} \displaystyle\sum_{v=-\infty}^{\infty} \sum_{m_1,\ldots,m_{p+1}=0}^{M-1} \sum_{m'_1,\ldots,m'_p=0}^{M-1} \sum_{m''_1,\ldots,m''_{i_1+i_2-2p}=0}^{M-1} \\[2em] \times \left(\displaystyle\int_0^{MT_s} \sum_{v=-\infty}^{\infty} \left(\prod_{j=1}^{p+1} g_{m_j}(t-vT_B) \prod_{j'=1}^{p} g^*_{m'_{j'}}(t-vT_B) \prod_{j''=1}^{i_1+i_2-2p} \left| g_{m''_{j''}}(t-vT_B) \right|^2 \right) dt \right) \\[2em] \times \left(\displaystyle\int_{-\infty}^{\infty} \prod_{j=1}^{p+1} g^*_{m_j}(t-\tau-vT_B) \prod_{j'=1}^{p} g_{m'_{j'}}(t-\tau-vT_B) e^{-j2\pi f\tau} d\tau \right) \end{array} \right)$$

$$\otimes \left(\sum_{k_1,\ldots,k_{p+1}=0}^{K-1} \sum_{k'_1,\ldots,k'_p=0}^{K-1} \delta\left(f - \frac{\left(\sum_{j=1}^{p+1} k_j - \sum_{j'=1}^{p} k_{j'} - \frac{K-1}{2} \right)}{T_s} \right) \right) \tag{30}$$

where

$$T_{i_1,i_2} = \binom{i_2+1}{p+1} \binom{i_1+1}{p+1} \binom{i_2}{p} \binom{i_1}{p} (p+1)!(p)!(i_2-p)!(i_1-p)!(\alpha\overline{p}_x)^{i_1+i_2+1}(K)^{i_1+i_2-2p} \frac{1}{MT_s}. \tag{31}$$

By defining $\tau' = t - \tau - vT_B$ and using linear convolution formula, (30) can be expressed as

$$\phi_{i_1,i_2}(f) = \sum_{p=0}^{\min(i_1,i_2)} T_{i_1,i_2}$$

$$\times \left[\begin{array}{c} \displaystyle\sum_{m_1,\ldots,m_{p+1}=0}^{M-1} \sum_{m'_1,\ldots,m'_p=0}^{M-1} \sum_{m''_1,\ldots,m''_{i_1+i_2-2p}=0}^{M-1} B(f) \\[2em] \times \left(G^*_{m_1}(f) \otimes \ldots \otimes G^*_{m_{p+1}}(f) \otimes G_{m'_1}(-f) \otimes \ldots \otimes G_{m'_p}(-f) \right) \end{array} \right]$$

$$\otimes \left(\sum_{k_1,\ldots,k_{p+1}=0}^{K-1} \sum_{k'_1,\ldots,k'_p=0}^{K-1} \delta\left(f - \frac{\left(\sum_{j=1}^{p+1} k_j - \sum_{j'=1}^{p} k_{j'} - \frac{K-1}{2} \right)}{T_s} \right) \right) \tag{32}$$

where $B(f)$ is equal to

$$
\begin{aligned}
B(f) &= \int\limits_{0}^{MT_s} \sum_{\upsilon=-\infty}^{\infty} \left(\prod_{j=1}^{p+1} g_{m_j}(t-\upsilon T_B) \prod_{j'=1}^{p} g^*_{m_{j'}'}(t-\upsilon T_B) \prod_{j''=1}^{i_1+i_2-2p} \left| g_{m_{j''}''}(t-\upsilon T_B) \right|^2 e^{-j2\pi f(t-\upsilon T_B)} \right) dt \\
&= \int\limits_{-\infty}^{\infty} \left(\prod_{j=1}^{p+1} g_{m_j}(t) \prod_{j'=1}^{p} g^*_{m_{j'}'}(t) \prod_{j''=1}^{i_1+i_2-2p} \left| g_{m_{j''}''}(t) \right|^2 e^{-j2\pi f(t)} \right) dt \\
&= \left(\begin{array}{l} G_{m_1}(f) \otimes ... \otimes G_{m_{p+1}}(f) \otimes G^*_{m_1'}(-f) \otimes ... \otimes G^*_{m_p'}(-f) \otimes \\[2mm] G^*_{m_1''}(-f) \otimes ... \otimes G^*_{m_{i_1+i_2-2p}''}(-f) \otimes G_{m_1''}(f) \otimes ... \otimes G_{m_{i_1+i_2-2p}''}(f) \end{array} \right).
\end{aligned}
\tag{33}
$$

By considering (32) and (33), $\phi_{i_1,i_2}(f)$ is obtained.

REFERENCES

[1] G. Wunder, P. Jung, M. Kasparick, T. Wild, F. Schaich, Y. Chen, S. T. Brink, I. Gaspar, N. Michailow, A. Festag, L. Mendes, N. Cassiau, D. Ktenas, M. Dryjanski, S. Pietrzyk, B. Eged, P. Vago, and F. Wiedmann, "5GNOW: Non-orthogonal, asynchronous waveforms for future mobile applications," *IEEE Commun. Mag.*, vol. 52, no. 2, pp. 97–105, Feb. 2014.

[2] J. Andrews, S. Buzzi, W. Choi, S. Hanly, A. Lozano, A. Soong, and J. Zhang, "What will 5G be?," *Selected Areas in Communications, IEEE Journal on,*, vol. 32, no. 6, pp. 1065–1082, June 2014.

[3] Ye Geoffrey Li and Gordon L Stuber, *Orthogonal frequency division multiplexing for wireless communications*, Springer Science & Business Media, 2006.

[4] S. A. Fechtel and A. Blaickner, "Efficient FFT and equalizer implementation for OFDM receivers," *IEEE Trans. Consum. Electron.*, vol. 45, no. 4, pp. 1104–1107, Nov. 1999.

[5] H. Kim, J. Kim, S. Yang, M. Hong, and Y. Shin, "An effective MIMO-OFDM system for IEEE 802.22 WRAN channels," *IEEE Trans. Circuits and Syst. II, Exp. Briefs*, vol. 55, no. 8, pp. 821–825, Aug. 2008.

[6] J. Van De Beek and F. Berggren, "Out-of-band power suppression in OFDM," *IEEE Commun. Lett.*, vol. 12, no. 9, pp. 609–611, Sep. 2008.

[7] B. Farhang-Boroujeny, "OFDM versus filter bank multicarrier," *IEEE Signal Process. Mag.*, vol. 28, no. 3, pp. 92–112, May. 2011.

[8] N. Michailow, M. Matth, I. S. Gaspar, A. N. Caldevilla, L. L. Mendes, A. Festag, and G. Fettweis, "Generalized frequency division multiplexing for 5th generation cellular networks," *IEEE Trans. Commun.*, vol. 62, no. 9, pp. 3045–3061, Sept. 2014.

[9] T. Ihalainen, A. Ikhlef, J. Louveaux, and M. Renfors, "Channel equalization for multi-antenna FBMC/OQAM receivers," *IEEE Trans. Veh. Technol.*, vol. 60, no. 5, pp. 2070–2085, Jun. 2011.

[10] R. Zakaria and D. Le Ruyet, "A novel filter-bank multicarrier scheme to mitigate the intrinsic interference: Application to MIMO systems," *IEEE Trans. Wireless Commun.*, vol. 11, no. 3, pp. 1112–1123, March 2012.

[11] G. Fettweis, M. Krondorf, and S. Bittner, "GFDM-Generalized Frequency Division Multiplexing," in *Proc. 69th IEEE VTC Spring, Barcelona, Spain*, Apr. 2009, pp. 1–4.

[12] N. Michailow, S. Krone, M. Lentmaier, and G. Fettweis, "Bit error rate performance of generalized frequency division multiplexing," in *proc. 76th IEEE VTC Fall, Quebec City, QC, Canada*, Sep. 2012, pp. 1–5.

[13] M. Matth, N. Michailow, I. Gaspar, and G. Fettweis, "Influence of pulse shaping on bit error rate performance and out of band radiation of generalized frequency division multiplexing," in *2014 IEEE International Conference on Communications Workshops (ICC)*, June 2014, pp. 43–48.

[14] I. Gaspar, N. Michailow, A. Navarro, E. Ohlmer, S. Krone, and G. Fettweis, "Low complexity GFDM receiver based on sparse frequency domain processing," in *Proc. 77th IEEE VTC spring, Dresden ,Germany,*, Jun. 2013, pp. 1–6.

[15] A. Farhang, N. Marchetti, and L. E. Doyle, "Low-complexity modem design for GFDM," *IEEE Trans. Signal Process.*, vol. 64, no. 6, pp. 1507–1518, March 2016.

[16] P. Reynaert and M. Steyaert, *RF power amplifiers for mobile communications*, Springer Science & Business Media, 2006.

[17] P. M. Lavrador, T. R. Cunha, P. M. Cabral, and J. C. Pedro, "The linearity-efficiency compromise," *IEEE Microwave Magazine*, vol. 11, no. 5, pp. 44–58, 2010.

[18] A. Mohammadi and F. M. Ghannouchi, *RF transceiver design for MIMO wireless communications*, vol. 145, Springer Science & Business Media, 2012.

[19] L. Sendrei and S. Marchevsk, "Nonlinear noise estimation and compensation in GFDM based communication systems for cognitive radio networks," in *Radioelektronika, 2015 25th International Conference*, April 2015, pp. 313–316.

[20] D. Schreurs, M. Odroma, A. A. Goacher, and M. Gadringer, *RF power amplifier behavioral modeling*, New York: Cambridge University Press, 2009.

[21] V. Tarokh, *New directions in wireless communications research*, Springer, 2009.

[22] K. G. Gard, H. M. Gutierrez, and M. B. Steer, "Characterization of spectral regrowth in microwave amplifiers based on the nonlinear transformation of a complex new Gaussian process," *IEEE Trans. Microwave Theory Tech.*, vol. 47, no. 7, pp. 1059–1069, Jul. 1999.

[23] E. Costa and S. Pupolin, "M-QAM-OFDM system performance in the presence of a nonlinear amplifier and phase noise," *IEEE Trans. Commun.*, vol. 50, no. 3, pp. 462–472, Mar. 2002.

[24] G. T. Zhou and R. Raich, "Spectral analysis of polynomial nonlinearity with applications to RF power amplifiers," *J. on Applied Signal Process, Special Issue on Nonlinear Signal and Image Process.*, vol. 2004, no. 12, pp. 1831–1840, 2004.

[25] M. M. Rahmati, A. Abdipour, A. Mohammadi, and G. Moradi, "An analytic approach for CDMA output of feedforward power amplifier," *Analog Integrated Circuits and Signal Processing*, vol. 66, no. 3, pp. 349–361, 2011.

[26] M. H. Madani, A. Abdipour, and A. Mohammadi, "Analysis of performance degradation due to non-linearity and phase noise in orthogonal frequency division multiplexing systems," *IET Commun.*, vol. 4, no. 10, pp. 1226–1237, July 2010.

[27] G. T. Zhou and J. S. Kenney, "Predicting spectral regrowth of nonlinear power amplifiers," *IEEE Trans. Commun.*, vol. 50, no. 5, pp. 718–722, May 2002.

[28] M. Majidi, A. Mohammadi, and A. Abdipour, "Accurate analysis of spectral regrowth of nonlinear power amplifier driven by cyclostationary modulated signals," *Analog Integrated Circuits and Signal Processing*, vol. 74, no. 2, pp. 425–437, 2013.

[29] E. Cottais, Y. Wang, and S. Toutain, "Spectral regrowth analysis at the output of a memoryless power amplifier with multicarrier signals," *IEEE Trans. Commun.*, vol. 56, no. 7, pp. 1111–1118, July 2008.

[30] M. Majidi, A. Mohammadi, and A. Abdipour, "Analysis of the power amplifier nonlinearity on the power allocation in cognitive radio networks," *IEEE Trans. Commun.*, vol. 62, no. 2, pp. 467–477, Feb. 2014.

[31] M. Baghani, A. Mohammadi, M. Majidi, and M. Valkama, "Analysis and rate optimization of ofdm-based cognitive radio networks under power amplifier nonlinearity," *IEEE Trans. Commun.*, vol. 62, no. 10, pp. 3410–3419, Oct. 2014.

[32] J. Staudinger, "Applying the quadrature modeling technique to wireless power amplifiers," *Microwave Journal*, vol. 40, no. 11, pp. 66–78, 1997.

[33] J. G. Proakis and M. Salehi, *Digital communications*, McGraw-Hill, 2008.

[34] R. Raich, *"Nonlinear system identification and analysis with applications to power amplifier modeling and power amplifier predistortion."*, Ph.D. thesis, School of Elect. Comput. Eng.,Georgia Inst. Technol., Atlanta, Mar. 2004.

[35] S. M. Kay, "Modern spectral estimation: theory and application," *Signal Processing Series*, 1988.

[36] I. S. Reed, "On a moment theorem for complex gaussian processes," *IEEE Trans. Inform. Theory*, vol. 3, no. 8, pp. 194–195, 1962.